PHYSICAL
CHEMISTRY

Measurement of Three-Dimensional Velocity Distributions of the Products of Cl$_2$, NO, and HCl Photodissociation or Photoionization

A. I. Chichinin*, T. Einfeld**, C. Maul**, and K.-H. Gericke**

Not long ago, it seemed unrealistic for molecular dynamics of photodissociation processes that the escape velocity and direction of photoproducts could be directly measured given an exact knowledge of the quantum states of these photoproducts and of the initial molecule. However, a breakthrough was made in 1987 with the advent of an imaging technique that made it possible to determine the three-dimensional spatial distribution of charged particles [1]. In this technique, resonance-enhanced multiphonon ionization (REMPI) is used for ionizing photofragments and the nascent fragment ions are accelerated by an electric field and detected as scintillations on a phosphorescent screen. Recently (1997), an improved version of this method—velocity map imaging [2, 3]—was suggested. In this method, due to the application of electrostatic lenses, all ions with the same initial velocity vector are mapped onto the same point on the detector irrespective of their initial positions.

In this paper, we describe a new version of the imaging technique, an alternative to velocity map imaging, in which a homogeneous electric field is used and a phosphorescent screen is exchanged for a delay-line detector (DLD) with high time resolution. This new method makes it possible to measure all three components of the velocity of a photodissociation or photoionization product. A setup consists of a time-of-flight mass spectrometer, a chamber for creating a molecular beam, and a laser system (Fig. 1). The mass spectrometer consists of a chamber with a homogeneous electric field, in which a molecular beam (the Y axis) and a laser beam (the X axis) intersect. Positive photoions created by laser radiation are accelerated by the electric field (along the Z axis) and are detected by means of the DLD.

* Institute of Chemical Kinetics and Combustion,
  Siberian Division, Russian Academy of Sciences,
  Institutskaya ul. 3, Novosibirsk, 630090 Russia
** Institut für Physikalische und Theoretische Chemie,
  Technische Universität Braunschweig,
  Hans-Sommer-Str. 10, D-38106 Braunschweig,
  Germany

The ion detecting system is a multichannel plate 8 cm in diameter, each channel of which is a photoelectron multiplier; the DLD is located behind this plate. In principle, such detectors have been known for half a century, but they have heretofore been used only in nuclear physics [4, 5]. The detector used in this work
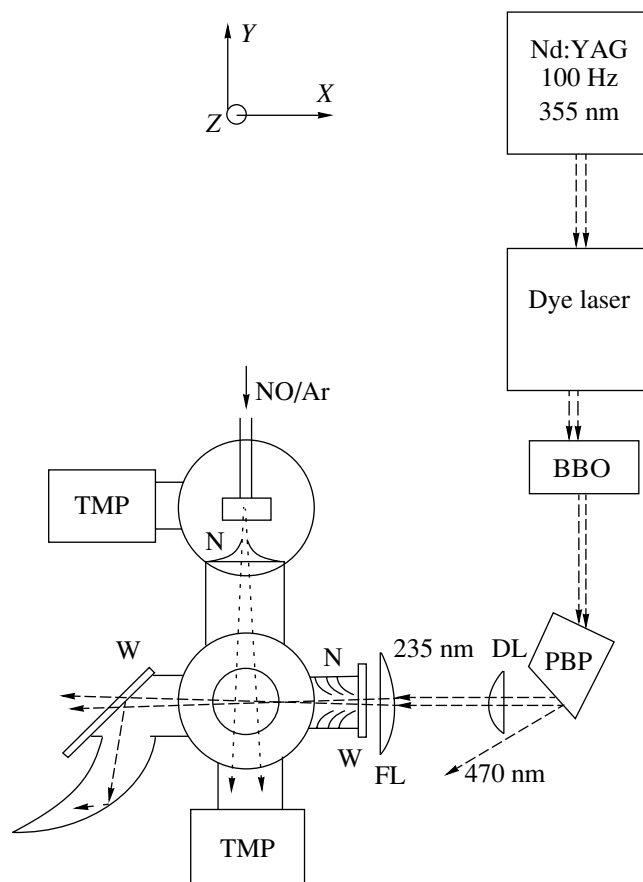

Fig. 1. Schematic of the experimental setup: TMP, turbomolecular pump; FL, focusing lens; DL, diverging lens; W, quartz window; N, nozzle; PBP, Pellin–Broca prism; BBO, crystal for frequency doubling.

was manufactured at the Institute of Nuclear Physics, University of Frankfurt [6]. The DLD is a ceramic frame, 10×10 cm, on which two wires, each 45 m long, are wound parallel to the X and Y axes. Each event—an ion or a photon that strikes the multichannel plate—produces charges on both delay lines. The idea of a DLD is that a charge appearing somewhere on the delay line is propagated in both directions toward the line ends, where the signal arrival time is recorded. Let X_1 and X_2 be these arrival times for the delay line along the X axis, and let Y_1 and Y_2 be such times for the delay line along the Y axis. The coordinates X and Y of an event in time units can be calculated as $(X_1 - X_2, Y_1 - Y_2)$, and the time of the event, which is the Z coordinate, can be calculated as $\dfrac{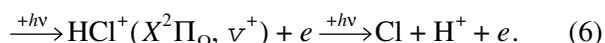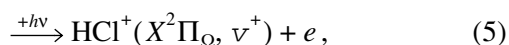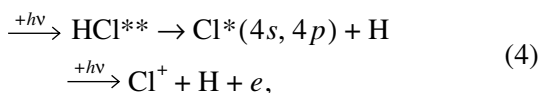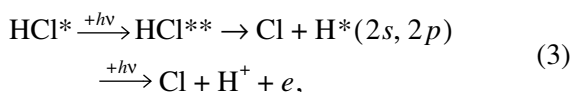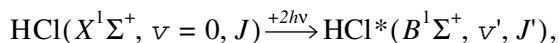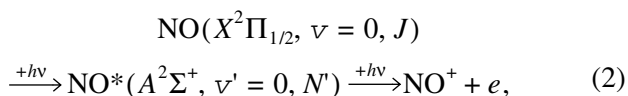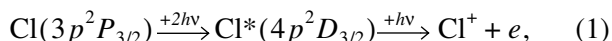X_1 + X_2 + Y_1 + Y_2}{4}$. The time of signal propagation from one end to the other is the same for both delay lines; therefore,

$$X_1 + X_2 = Y_1 + Y_2.$$

Only the signals that meet this condition are taken into account; the other signals are ignored.

Mention should be made of methodical experiments in which a source of α particles was placed in the chamber of the mass spectrometer and a metallic wire was located before the DLD. From analysis of the image of this wire on the DLD, its spatial resolution was determined to be 0.4 mm.

The laser system consists of an Nd:YAG laser and a dye laser. The dye laser fundamental is first doubled and then focused into the mass spectrometer chamber. In this work, we obtained $(2 + 1_i)$ REMPI spectra [7, 8] of a Cl atom (235.336 nm) and an HCl molecule (transitions at about 237 nm); $(1 + 1_i)$ REMPI spectra [9] of an NO molecule (about 226.2 nm); and $(2+1+1_i)$ and $(2 + 1_i + 1)$ REMPI spectra [8, 10] of H^+ and Cl^+ ions (the subscript index designates the ionizing photon):

$$Cl(3p^2P_{3/2}) \xrightarrow{+2h\nu} Cl^*(4p^2D_{3/2}) \xrightarrow{+h\nu} Cl^+ + e, \quad (1)$$

$$NO(X^2\Pi_{1/2}, v = 0, J)$$
$$\xrightarrow{+h\nu} NO^*(A^2\Sigma^+, v' = 0, N') \xrightarrow{+h\nu} NO^+ + e, \quad (2)$$

$$HCl(X^1\Sigma^+, v = 0, J) \xrightarrow{+2h\nu} HCl^*(B^1\Sigma^+, v', J'),$$

$$HCl^* \xrightarrow{+h\nu} HCl^{**} \to Cl + H^*(2s, 2p)$$
$$\xrightarrow{+h\nu} Cl + H^+ + e, \quad (3)$$

$$\xrightarrow{+h\nu} HCl^{**} \to Cl^*(4s, 4p) + H$$
$$\xrightarrow{+h\nu} Cl^+ + H + e, \quad (4)$$

$$\xrightarrow{+h\nu} HCl^+(X^2\Pi_\Omega, v^+) + e, \quad (5)$$

$$\xrightarrow{+h\nu} HCl^+(X^2\Pi_\Omega, v^+) + e \xrightarrow{+h\nu} Cl + H^+ + e. \quad (6)$$

Temperatures of molecular beams for different buffer gases

Gas	V_{max}, m/s	v_{exp}, m/s	T_Y, K	T_{rot}, K	T_{calcd}, K
Ar	554	558 ± 4	3.5 ± 0.5	3.0 ± 0.5	-4 ± 5
He	1751	1718 ± 12	12.3 ± 2	8 ± 2	11 ± 5
N_2	783	747 ± 12	12.7 ± 2	12 ± 2	26 ± 9
H_2	2931	2041 ± 40			152 ± 6

Here, v stands for vibrational and N and J, for rotational quantum numbers. It is worth noting that HCl^+, Cl^+, and H^+ ions are detected in processes (3)–(6). This new type of measurement is referred to as mass-resolved REMPI [10].

The possibilities of this method are illustrated by experiments on molecular beam imaging. Figure 2 shows three distributions of NO^+ ions at different times of flight. Analysis of spatial distributions of NO along the Y axis showed that these distributions $W(y)$ have a Gaussian shape:

$$W(y) \sim \exp\left(-\ln 2\left[\frac{2(y - L)}{W_s}\right]^2\right),$$

where L is the position of the molecular beam maximum and W_s is the width of this spatial distribution. The lowest W_s value obtained in similar experiments is ~1 ns, which is the time resolution of this method. The L value is a linear function of the time of flight t_0, $L = L_0 + v_{exp}t_0$ (here, L_0 is the position of the maximum of the background signal of NO molecules). The molecular beam velocity $v_{exp} = \dfrac{dL}{dt_0}$ is determined from the slope of the plot of L versus t_0 (table).

Let us introduce T_Y as the translational temperature of the beam along the Y axis

$$W(v_y) = W_y \exp\left[-\frac{M_{NO}(v_y - v_{exp})^2}{2kT_Y}\right],$$

where v_y and M_{NO} are, respectively, the velocity and mass of the NO molecule. Substituting $v_y - v_{exp} = \dfrac{y - L}{t_0}$, we find the following relationship between W_s and T_Y:

$$T_Y = \frac{M_{NO}\left(\dfrac{dW_s}{dt_0}\right)^2}{8k\ln 2},$$

where $\dfrac{dW_s}{dt_0}$ is the slope of a linear function that fits the experimental dependence of W_s on t_0.
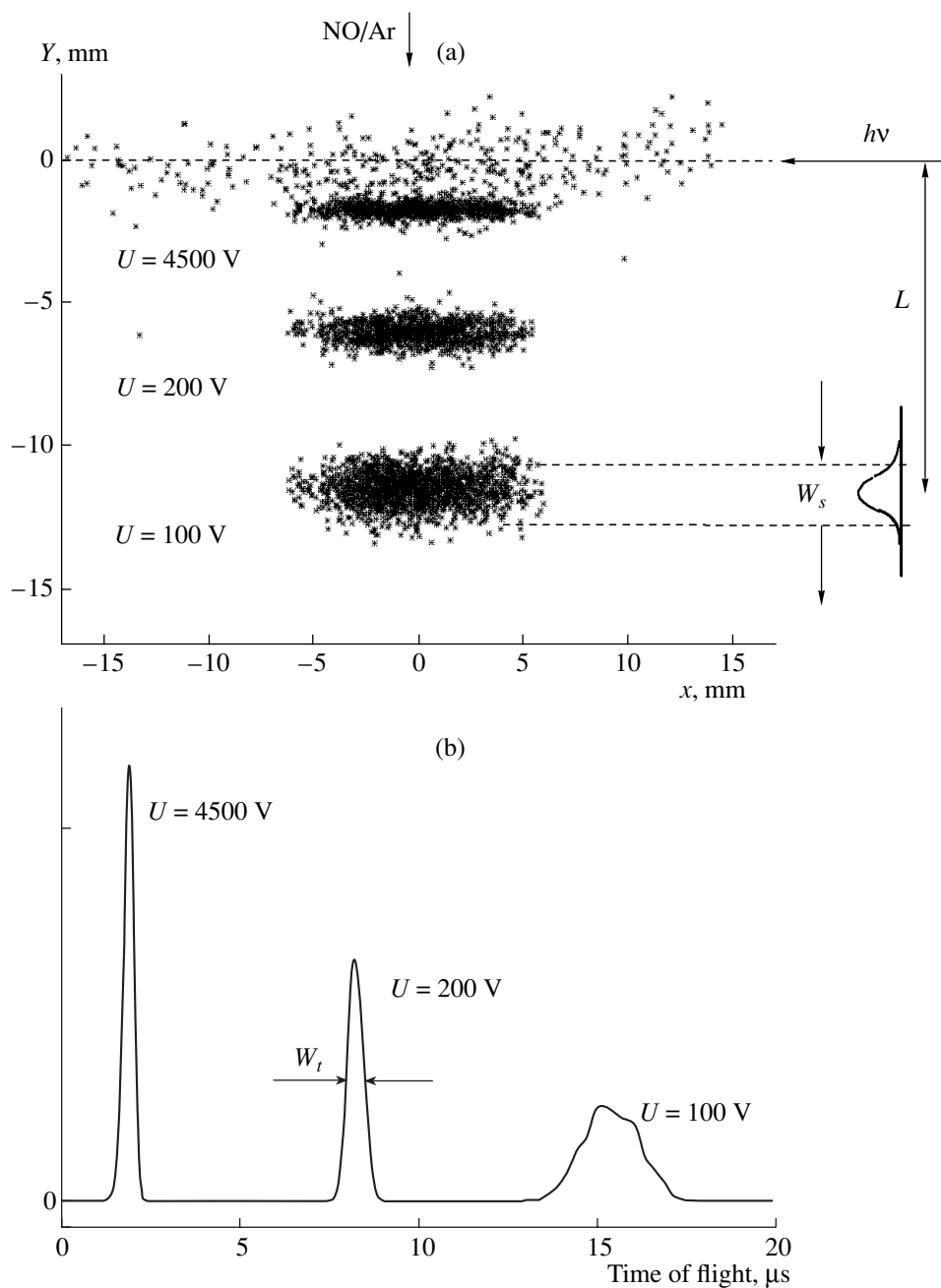
Fig. 2. Experiments with NO/Ar beams. (a) Spatial distribution of NO^+ ions at different times of flight (accelerating voltages U). The upper wide and long distribution arises from background hot NO molecules. (b) Time-of-flight distributions obtained for the same three groups of ions and shown in the same plot. For clarity, the widths W_t of the time-of-flight distributions are increased 100-fold.

The internal beam temperature T_{calc} can be calculated by the formula

$$T_{calc} = T_0\left[1 - \left(\frac{v_{exp}}{v_{max}}\right)^2\right].$$

Here, v_{max} is the theoretically calculated maximum possible beam velocity [11],

$$v_{max} = \sqrt{\frac{\gamma}{\gamma - 1}}\sqrt{\frac{2kT_0}{M_B}},$$

where M_B is the molecular mass of a buffer gas; k is the Boltzmann constant; $T_0 = 295$ K is room temperature; and $\gamma = \dfrac{C_P}{C_V}$, with γ being $\dfrac{5}{3}$ and $\dfrac{7}{5}$ for, respectively, monatomic and diatomic buffer gases.
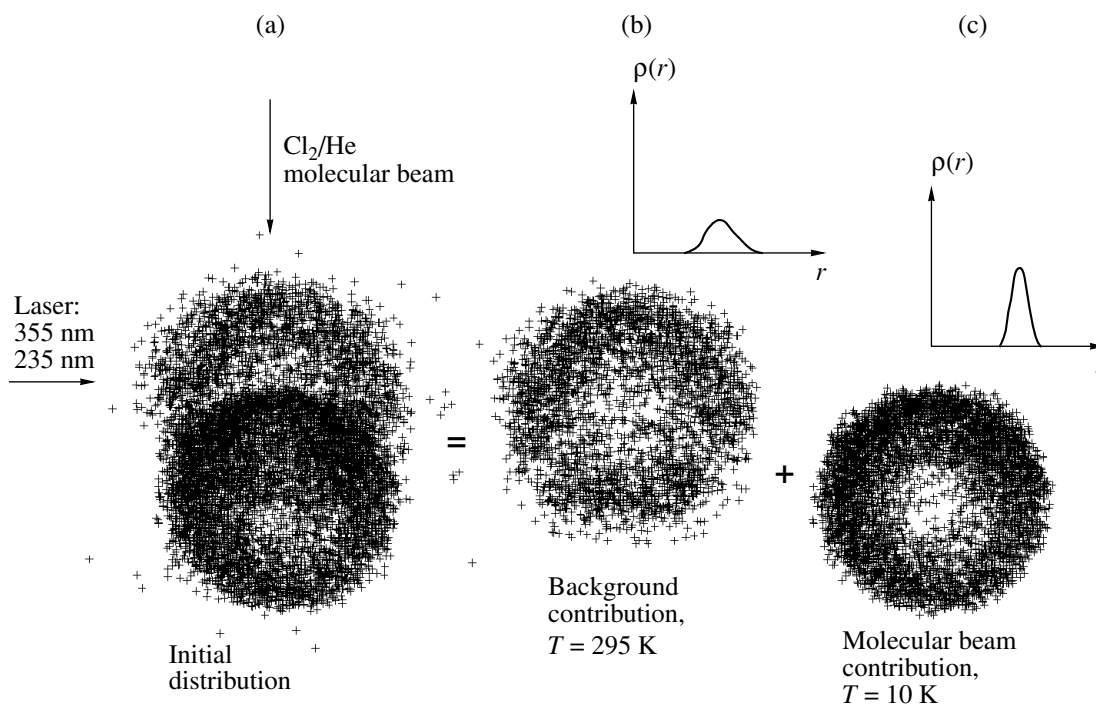
Fig. 3. Photolysis of Cl_2 at 355 nm. (a) The three-dimensional velocity distribution of Cl atoms consists of two spherical distributions due to hot and cold molecules. (b, c) Schematic of the procedure of separation of a distribution. For each distribution, the radial distribution function is shown.

The rotational temperature T_{rot} of NO molecules was routinely measured from the intensities of REMPI lines of the electronic rotational spectrum.

It is worth noting that all three temperatures—T_{rot}, T_{exp}, and T_Y—are of different nature and can be different. However, these temperatures are roughly the same in our case (table).

Studying three-dimensional spherical distributions is exemplified by the photodissociation $Cl_2 + h\nu \rightarrow 2Cl(^2P_{3/2})$. In these experiments, the $Cl(^2P_{3/2})$ atoms are ionized according to scheme (1) 3 ns after the photolysis of a Cl_2/He mixture by radiation with $\lambda = 355$ nm. The experimental three-dimensional distribution of Cl atoms consists of two intersecting spherical distributions (Fig. 3). One of them corresponds to background hot Cl_2 molecules and the other, to cold molecules from the molecular beam. Both distributions have a Gaussian shape, with the width at half-maximum being 0.22 and 0.53 km/s for the cold and hot Cl_2 molecules, respectively. The width of similar distributions is mainly determined by the translational and rotational temperatures of the Cl_2 molecule, the laser spot length, the spatial resolution of a DLD, and the laser pulse width (5 ns). It is worth noting that the best resolution of the method is achieved when the molecular beam is as cold as possible and a two-lens configuration and a large image diameter are used.

The configuration with two lenses suggested in this work is an alternative to the velocity map imaging method [2, 3]. In this configuration, the laser beam is slightly expanded with the first diverging lens and then focused with the second lens (Fig. 1). The focal lengths of the lenses and the distances between them were optimized by calculations that included aberration and diffraction. According to calculations, this configuration allows one to make the laser spot length negligible (~0.2 mm).

The time and energy resolution of the method is illustrated by experiments on studying the ionization of NO and HCl molecules. The change in the momentum of a molecule in the course of photoionization is usually ignored; however, our method has a very high energy resolution (10 μeV), which allows one to study photoionization by observing ions rather than electrons. Figure 4 shows the REMPI signals of NO^+ ions recorded in experiments with different laser polarizations: $E \perp Z$ and $E \parallel Z$, where E is the electric field of laser radiation. The same figure also shows the time intervals $t_0 \pm \Delta t$, where t_0 is the mean time of flight and Δt is determined by the electron recoil that arises from the escape of an electron from a molecule in the course of photoionization. This quantity has a simple meaning: ions with initial velocities v_0 and $-v_0$ along the Z axis arrive at the moments of time $t_0 - \Delta t$ and $t_0 + \Delta t$, respectively. Here, $v_0 = 14.1$ m/s is the velocity of the NO^+ ion,

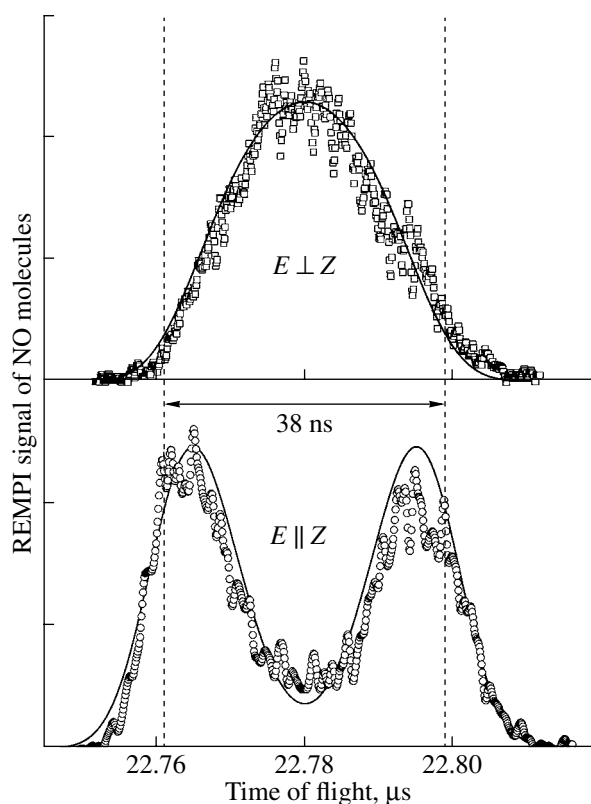$$v_0 = \frac{m_e}{M_{NO}} \sqrt{\frac{2(2h\nu - I_{NO})}{m_e}},$$

Fig. 4. Velocity distribution of NO molecules resulting from electron recoil in the course of photoionization. The time interval $t_0 \pm \Delta t$ is shown by vertical dashed lines. Solid curves show the result of fitting the theoretical expression with $\beta_2 = 2.0 \pm 0.2$ and $\beta_4 = 0$ to the experimental data points.

where m_e is the mass of an electron, M_{NO} is the mass of an ion, $h\nu$ is the photon energy, and I_{NO} is the ionization potential of NO molecules. The interval Δt can be calculated as $\Delta t = \dfrac{v_0}{a}$, where a is the acceleration of NO$^+$ ions in an electric field with the strength E_{ex}, $a = \dfrac{eE_{ex}}{M_{NO}}$.

The angular distribution of NO$^+$ ions in this case is described by the expression [13, 14]

$$I(\theta) = \frac{\sin\theta}{4\pi}[1 + \beta_2 P_2(\cos\theta) + \beta_4 P_4(\cos\theta)], \quad (7)$$

where P_2 and P_4 are Legendre polynomials, θ is the polar spherical angle measured from the direction of the vector E, and β_2 and β_4 are anisotropy parameters. From this, expressions for time-of-flight distributions of ions can be obtained, which were used for fitting the experimental data (Fig. 4).

It is important that the time distribution of NO$^+$ ions is adequately described by Eq. (7), which implies that all ions have velocity v_0. However, a radically different distribution was obtained for HCl$^+$ ions. This distribution was simulated using a distribution of ions by velocity v_0; hence, we obtained the distribution of HCl$^+$ ions with respect to vibrational number v^+ in the course of ionization (5). As a result, we obtained a method of studying photoionization that is an alternative to photoelectron spectroscopy.

It should be emphasized that this three-dimensional method is much more informative than two-dimensional imaging methods [1, 12]. For example, in this work, the β_2 parameters for H$^+$ ions that form in process (3) were found to be 1.2 and 0.7 for $J' = J'' = 0$ and $J' = J'' = 1$, respectively, and to be slightly different for $E \perp Z$ and $E \parallel Z$. Thus, four β_2 parameters were measured and two quantities were calculated from them, namely, the degree of alignment of HCl* molecules in process (2) and the degree of alignment of HCl molecules in the molecular beam [15]. A two-dimensional technique provides two β_2 parameters and, hence, allows one to study only one type of alignment.

REFERENCES

1. Chandler, D.W. and Houston, P.L., *J. Chem. Phys.*, 1987, vol. 87, no. 2, pp. 1445–1447.
2. Eppink, A.T.J.B. and Parker, D.H., *Rev. Sci. Instrum.*, 1997, vol. 68, no. 9, pp. 3477–3484.
3. Parker, D.H. and Eppink, A.T.J.B., *J. Chem. Phys.*, 1997, vol. 107, no. 7, pp. 2357–2362.
4. Lampton, M., Siegmund, O., and Raffanti, R., *Rev. Sci. Instrum.*, 1987, vol. 58, no. 12, pp. 2298–2305.
5. Sobottka, S.E. and Williams, M.B., *IEEE Trans. Nucl. Sci.*, 1988, vol. 35, no. 1, pp. 348–351.
6. Jagutzki, O., Mergel, V., Ullmann-Pfleger, K.U., *et al.*, *Nucl. Instrum. Methods Phys. Res. A*, 2002, vol. 477, no. 113, pp. 244–249.
7. Arepalli, S., Presser, N., Robie, D., and Gordon, R.J., *Chem. Phys. Lett.*, 1985, vol. 118, no. 1, pp. 88–92.
8. Kvaran, A., Logadottir, A., and Wang, H., *J. Chem. Phys.*, 1998, vol. 109, no. 14, pp. 5856–5867.
9. Danielak, J., Domin, U., Kepa, R., *et al.*, *J. Mol. Spectrosc.*, 1997, vol. 181, pp. 394–402.
10. Spiglanin, T.A., Chandler, D.W., and Parker, D.H., *Chem. Phys. Lett.*, 1987, vol. 137, no. 5, pp. 414–420.
11. Miller, D.R., in *Atomic and Molecular Beam Methods*, G. Scoles, Ed., New York: Oxford Univ. Press, 1988, part 1, p. 14.
12. Whitaker, B., *Imaging in Molecular Dynamics: Technology and Applications*, Cambridge: Cambridge Univ. Press, 2003.
13. Dixit, S.N., Lynch, D.L., McKoy, V., and Huo, W.M., *Phys. Rev. A*:, 1985, vol. 32, no. 2, pp. 1267–1270.
14. Leahy, D.J., Reid, K.L., and Zare, R.N., *J. Chem. Phys.*, 1991, vol. 95, no. 3, pp. 1757–1767.
15. Pirani, F., Cappelletti, D., Bartolomei, M., *et al.*, *Phys. Rev. Lett.*, 2001, vol. 86, pp. 5035–5038.